IMMUNOLOGY

Harnessing T cell exhaustion and trogocytosis to isolate patient-derived tumor-specific TCR

Francesco Manfredi[1], Lorena Stasi[1], Silvia Buonanno[1], Francesca Marzuttini[1], Maddalena Noviello[1], Sara Mastaglio[2], Danilo Abbati[1], Alessia Potenza[1], Chiara Balestrieri[1,3], Beatrice Claudia Cianciotti[1], Elena Tassi[1], Sara Feola[4], Cristina Toffalori[5], Marco Punta[3,5], Zulma Magnani[1], Barbara Camisa[1], Elena Tiziano[1], Maria Teresa Lupo-Stanghellini[2], Rui Mamede Branca[6], Janne Lehtiö[6], Tiina M. Sikanen[7], Markus J. Haapala[7], Vincenzo Cerullo[4], Monica Casucci[8], Luca Vago[2,5,9], Fabio Ciceri[2,8], Chiara Bonini[1,8]*†, Eliana Ruggiero[1]*†

To study and then harness the tumor-specific T cell dynamics after allogeneic hematopoietic stem cell transplant, we typed the frequency, phenotype, and function of lymphocytes directed against tumor-associated antigens (TAAs) in 39 consecutive transplanted patients, for 1 year after transplant. We showed that TAA-specific T cells circulated in 90% of patients but display a limited effector function associated to an exhaustion phenotype, particularly in the subgroup of patients deemed to relapse, where exhausted stem cell memory T cells accumulated. Accordingly, cancer-specific cytolytic functions were relevant only when the TAA-specific T cell receptors (TCRs) were transferred into healthy, genome-edited T cells. We then exploited trogocytosis and ligandome-on-chip technology to unveil the specificities of tumor-specific TCRs retrieved from the exhausted T cell pool. Overall, we showed that harnessing circulating TAA-specific and exhausted T cells allow to isolate TCRs against TAAs and previously not described acute myeloid leukemia antigens, potentially relevant for T cell–based cancer immunotherapy.

INTRODUCTION

In patients affected by blood malignancies, allogeneic hematopoietic stem cell transplantation (allo-HSCT) is able to eradicate or contain cancer cells surviving chemoradiotherapy (*1*). However, tumors can evade the newly imposed immune pressure (*2*) by shaping T cell functionality (*3*). While functional, long-lasting tumor specific T cells are associated with durable tumor control (*4*, *5*), suboptimally stimulated, exhausted T cells may concur to disease relapse (*6*–*8*). Exhausted T cells express inhibitory receptors (IRs) (*3*) and progressively lose effector functions, so that a higher number of IRs and a lower expression of activation markers translate into greater T cell dysfunction (*9*). In blood malignancies, T cells up-regulate IRs at relapse (*10*), while IR ligands have been detected on blasts (*11*). In particular, minor-histocompatibility antigen-specific T cells (*12*) and bone marrow–infiltrating stem cell memory T cells (T_{SCM}), antigen-experienced T cells with self-renewal abilities central for long-term memory maintenance (*13*, *14*), have been shown to express a variety of IRs at relapse (*10*). The efficacy of immune checkpoint inhibitors in reinvigorating graft-versus-leukemia (GvL) further underlined the relevance of exhaustion in tumor escape but also underscored that alloreactive T cells could express IRs, because graft-versus-host disease (GvHD) may ensue with this therapy (*15*, *16*). Together, these results warrant further studies to elucidate which IRs shape the fate of tumor-specific T cells.

Adoptive T cell therapy (ACT) relies on tumor antigen-specific T cells to eliminate cancer cells. ACT can exert GvL with reduced GvHD risk, as underlined by the efficacy of ACT using T cells engineered to target the tumor-associated antigen (TAA) New York esophageal squamous cell carcinoma-1 (NY-ESO-1) in multiple myeloma (*17*) and Wilms′s tumor 1 (WT1) in acute leukemia (*5*). TAAs are perhaps the most characterized antigen class, and cytotoxic T lymphocytes directed against a number of TAAs, such as enhancer of zeste homologue 2 (EZH2) (*18*), melanoma antigen gene A2 (MAGE-A2) (*19*), human telomerase reverse transcriptase (hTERT) (*20*), survivin (*21*), proteinase 3 (PR3) (*22*), preferentially expressed antigen of melanoma (PRAME) (*23*) and WT1 (*24*), have been indeed detected in hematological patients (*25*). Nonetheless, the direct therapeutic exploitation of ex vivo expanded TAA-specific T cells has been limited (*26*, *27*), as a sufficiently high number of TAA-specific T cells for clinical purposes are rarely obtained. The full exploitation of these target antigens could benefit from the isolation of functional T cell receptors (TCRs) specific for the epitopes of interest to be then used in the context of T cell engineering (*28*). Different technologies have been proposed to identify previously unknown TAA-specific TCRs, whose efficacy and peptide specificity remain often poorly validated (*29*, *30*). A better knowledge of the tumor-specific T cell phenotype could help to tackle this issue,

[1]IRCCS San Raffaele Scientific Institute, Division of Immunology, Transplantation, and Infectious Diseases, Experimental Hematology Unit, via Olgettina 60, Milan 20132, Italy. [2]IRCCS San Raffaele Scientific Institute, Hematology and Hematopoietic Stem Cell Transplantation Unit, via Olgettina 60, Milan 20132, Italy. [3]Center for Omics Sciences, IRCCS San Raffaele Scientific Institute, via Olgettina 60, Milan 20132, Italy. [4]University of Helsinki, ImmunoVirotherapy Lab, Yliopistonkatu 4, 00100 Helsinki, Finland. [5]IRCCS San Raffaele Scientific Institute, Division of Immunology, Transplantation and Infectious Disease, Unit of Immunogenetics, Leukemia Genomics and Immunobiology, via Olgettina 60, Milan 20132, Italy. [6]Science for Life Laboratory, Department of Oncology-Pathology, Karolinska Institute, 171 65 Solna, Sweden. [7]Drug Research Program, Faculty of Pharmacy, Division of Pharmaceutical Chemistry and Technology, Helsinki University,, Viikinkaari 5E, 00014 Helsinki, Finland. [8]IRCCS San Raffaele Scientific Institute, Division of Immunology, Transplantation and Infectious Disease, Innovative Immunotherapies Unit, via Olgettina 60, Milan 20132, Italy. [9]Vita Salute San Raffaele University, Milan, Italy.
*Corresponding author. Email: ruggiero.eliana@hsr.it (E.R.); bonini.chiara@hsr.it (C. B.)
†These authors contributed equally to this work.

defining the sampling time point and the phenotype to pinpoint a T cell subset enriched in tumor specificity.

With the aim of elucidating and harnessing the dynamic landscape of circulating tumor-specific lymphocytes, TAA-specific T cells were longitudinally evaluated in 39 consecutive patients affected by hematological malignancies, up to 1 year after allo-HSCT. We showed that T cells specific for different TAAs circulate in patients, display a distinctive phenotypic signature that link exhaustion to disease relapse risk, and, despite expressing IRs, harbor functional TCRs. We then demonstrated that IRs can be exploited to isolate functional tumor-specific TCRs and that the specificity of orphan TCRs can be unveiled by trogocytosis (*31*) typing and PeptiChip (*32*) analysis.

RESULTS

Deeply exhausted TAA-specific T_{SCM} cells accumulate before disease relapse

The occurrence of TAA-specific T cells was studied in the peripheral blood of 39 consecutive patients affected by hematological malignancies and treated with allo-HSCT and post-transplant cyclophosphamide, for up to 1 year or until detection of a positive measurable residual disease (MRD; Table 1). The tumor T cell response was assessed by profiling lymphocytes restricted for EZH2, MAGE-A2, hTERT, survivin, PR3, PRAME, and WT1-derived immunogenic peptides, mounted on human leukocyte antigen (HLA)–A*0201, A*0301 and A*2402 restrictions, widely expressed by the Caucasian population. TAA-specific cells were quantified by flow cytometry, before conditioning and at 30 to 45, 60, 90, 120 to 150, 180, and 365 days after allo-HSCT (n = 322 samples). To have a reference of functional, long-lasting antigen-specific T cells, cytomegalovirus (CMV)–specific T cells restricted for the same HLAs and one immunodominant epitope per HLA were analyzed (n = 91 samples, fig. S1A and table S1 and S2). Thanks to an optimized staining (*33*, *34*) and analysis protocol (*35*, *36*), TAA-specific T cell detection was efficient and specific (figs. S1B, S2, and S3). Thirty-five of 39 (90%) tested patients showed circulating TAA-specific T cells in at least one time point, on average with three out of four dextramers used (75%, fig. S4A), while 33 of 39 (85%) screened patients were positive for CMV-specific dextramers. In median, TAA-specific T cells circulated in the n = 322 samples at 0.31 cells/μl (0.08% of total circulating $CD8^+$ T cells), while CMV-specific T cells were more frequent (1.32 cells/μl, 0.40%; Fig. 1, A and B, and fig. S4B). CMV-specific cells increased soon after transplant, tailing the timing of CMV reactivation (median, 90 days) after allo-HSCT, while tumor-specific CD8 T cells enriched later and persisted up to 1 year after transplant (Fig. 1C and fig. S4C). TAA-specific T cells were undetectable in the peripheral blood of the majority of healthy donors tested (fig. S5). In addition, we failed to consistently detect myeloid-derived TAA-specific T cells in patients affected by lymphoid malignancies and viceversa (fig. S6). Overall, these observations indicate that in vivo priming occurring in patients is required to sustains the expansion of TAA-specific T cells. We then evaluated the memory differentiation and the expression of inhibitory (2B4, TIM-3, CD39, LAG3, PD1, and KLRG1) and activation markers (CD25, GITR, and HLA-DR; fig. S7) on TAA-specific T cells and compared them to total $CD8^+$ and CMV-specific T cells. TAA-specific T cells preferentially accumulated early differentiated T_{SCM} ($CD45^+CD62L^+CD95^+$) cells rather than effector memory (T_{EM}, $CD45^-CD62L^-$), terminal effector ($T_{EM}RA$, $CD45^+CD62L^-$), or central memory (T_{CM}, $CD45^-CD62L^+$) T cells early after allo-HSCT (Fig. 1D and fig. S8A) and were more exhausted, overexpressing KLRG1 (Fig. 1E) and, at selected time points, PD1 (days +90 and +120.150) and TIM3 (day +90 and +365; fig. S8B). These results were independent from GvHD onset (fig. S9) and disease status at transplant (fig. S10). To comprehensively evaluate the interplay between exhaustion, memory, and activation in the different time points after allo-HSCT, events were segregated according to multiple markers expression via cytoChain unsupervised dimensionality reduction and clustering (*36*) (Fig. 1F). Discrete areas (clusters) preferentially enriched with either CMV-specific or TAA-specific T cells from a relevant fraction of patients, and clusters representing CMV-specific T cells expressed little IRs, while clusters containing TAA-specific T cells were either akin to CMV ones (clusters 5-11-21) or coexpressed multiple IRs (clusters 42 and 48; Fig. 1G and fig. S11, A and B). IR coexpression was higher for TAA-specific T cells across different time points (Fig. 1H) but was differentially associated with activation markers as time passed. Early after allo-HSCT (<120 days), IRs were already detectable but expressed with CD25 and/or HLA-DR, a phenotype compatible with recently activated T cells, while at later time points (≥120 days), IRs were coexpressed alone, suggesting exhaustion (fig. S11C). We could also define a TAA-specific signature on the basis of cluster 48 markers expression, representing deeply exhausted early memory precursors ($CD45RA^+CD62L^+CD95^+$ $TIM3^+2B4^+PD1^+KLRG1^+$, exhausted-T_{SCM} signature; fig. S12A) negative for activation markers (fig. S12B), and more represented in TAA-specific T cells (fig. S12C).

We next investigated whether an accumulation of exhausted TAA-specific T cell subset could be a premature sign of relapse after allo-HSCT. We observed that patients eventually experiencing relapse (REL) accumulated TAA-specific T_{SCM} cells (fig. S12D), expressed selected IRs at higher frequency (fig. S12E) and coexpressed more IRs (Fig. 1I) than patients who achieved long-term disease remission [complete remission (CR)]. In addition, in REL patients, the exhausted-T_{SCM} signature was more frequent (Fig. 1J and fig. S12F) and was a more consistent part of the TAA-specific T_{SCM} population (fig. S12G) than in CR. The TAA-specific T cell dynamics were also different, as in REL patient TAA-specific cells contracted after an initial expansion burst (Fig. 1K). We saw no reduced WT1 overexpression and no evidence of antigen loss in blasts at relapse in the N = 5 WT1-positive relapse samples of our cohort (fig. S13A) and in a confirmatory cohort of N = 32 diagnosis-relapse sample pairs (fig. S13B).

Overall, these results indicate that exhaustion is a feature of TAA-specific T cells, in particular for patients who will subsequently experience disease relapse. Already before relapse, deeply inhibited T_{SCM} cells accumulate, exhaustion deepens, and TAA-specific cells are progressively lost despite antigen persistence.

Hypofunctional TAA-specific T cells harbor functional TAA-directed TCRs

To evaluate the cytolytic activity of TAA-specific lymphocytes, we sorted and activated hTERT-, MAGE-A2–, survivin-, and WT1-specific T cells (fig. S14A) from patients showing circulating TAA-specific T cells, isolating 16 TAA-specific cell cultures from 10 of 16 patients tested (Fig. 2A). Despite dextramer enrichment (fig. S14B), no specific lysis, degranulation, nor inflammatory

Table 1. Clinical characteristics of the patient cohort. AML, acute myeloid leukemia; MDS, myelodysplasia; CML, chronic myelogenous leukemia; ALL, acute lymphoid leukemia; CLL, chronic lymphoid leukemia; HSCT, hematopoietic stem cell transplantation; CR, complete remission; CMV, cytomegalovirus; aGvHD, acute graft-versus-host disease; cGvHD, chronic graft-versus-host disease.

	Number of patients (%)
Disease type	
AML	20 (52)
MDS	4 (10)
CML	4 (10)
ALL	4 (10)
CLL	1 (3)
Multiple myeloma	2 (5)
Non-Hodgkin lymphoma	4 (10)
Caucasic origin	
No	6 (15)
Yes	33 (85)
Chimerism at day 30 (% of host)	
≤0.1	5 (13)
$0.1 \leq \times \leq 1$	20 (52)
$1 \leq \times \leq 10$	12 (30)
≥10	2 (5)
Disease remission status at allo-HSCT	
CR1	17 (44)
CR > 1	11 (28)
Active/progressive disease	11 (28)
Transplant type	
Haploidentical/mismatched related donor (MMRD)	13 (33)
Matched-related donor (MRD)	5 (13)
Matched-unrelated donor (MUD)	19 (49)
Cord blood (CB)	2 (5)
Donor-patient relationship (% of total MMRD plus MRD)	
Parent to children	2 (11)
Children to parent	3 (17)
Nephew to grandparent	2 (11)
Siblings	11 (61)
CMV host (H)–donor (D) status	
H+D+	29 (74)
H+D−	9 (23)
H−D+	1 (3)
H−D−	0 (0)
CMV reactivation	
No	19 (49)
Yes	20 (51)
Time from HSCT to CMV reactivation (median, IQR)	90, 30–90
GvHD prophylaxis	
PTCy/Rapa	6 (15)
PTCy/Rapa/MMF	33 (85)
aGvHD incidence	
None	24 (62)

continued on next page

	Number of patients (%)
Overall <2	2 (5)
Overall ≥2	13 (33)
Time to HSCT to aGVHD occurrence (median, IQR)	60, 45–90
cGvHD incidence	
None	20 (51)
Mild	4 (10)
Moderate	9 (23)
Severe	6 (16)
Time from HSCT to cGvHD occurrence (median, IQR)	150, 60–240
Disease status at last follow-up	
Complete remission	30 (77)
Relapse	9 (23)
Median interval to relapse (median, IQR)	180, 157–625
Median clinical follow-up (median, IQR)	839, 349–956
Mean clinical follow-up (mean, SD)	629, 341

cytokine production was detected when expanded T cells were cocultured with peptide-pulsed T2 tumor cell lines (174xCEM.T2, ATCC-CRL-1992) (fig. S15, A to C). We then questioned whether this observation could be explained by exhaustion or by low TCR avidity. To address this issue, we reconstructed (*37*) the α and β TCR sequences from dextramer$^+$ T cell cultures. All cultures were composed by a limited amount of TCR clones, with reduced clonal diversity compared to ex vivo T cells (Fig. 2B), allowing α-β pairing and assembly of N = 18 dominant TCRs reactive against WT1, MAGE-A2, survivin, and hTERT epitopes. The TCRs were then engineered into TCR-KO (knockout) donor T cells (*38*) (fig. S15, D and E) to generate TCR-edited cells (fig. S15F) that were challenged against tumor cell lines pulsed with the appropriate peptides. All constructs but Pt#3 WT1#1 and Pt#12 MAGE-A2#1-2 induced apoptosis of target cells, at different magnitude (Fig. 2C and fig. S15G). In addition, many edited T cells degranulated and produced proinflammatory cytokines in response to peptide-pulsed cell lines (fig. S16, A and B) and mediated peptide-specific target killing (Fig. 2D). We then challenged the most promising constructs (n = 14) against primary acute myeloid leukemia (AML) blasts. Edited T cells were cocultured with WT1-, hTERT- or survivin-overexpressing primary AML blasts, either exhibiting (target blasts) or not (control blasts) the relevant HLA restriction (HLA-A*0201$^+$ targets for $WT1_{37–45}$ (*39*) and $survivin_{96–104}$; HLA-A*0301$^+$ targets for $hTERT_{663–672}$). Apoptosis was induced (Fig. 2E and fig. S16C) and target blasts were eliminated (Fig. 2F) by 12 of 14 tested engineered cellular products, while a number of constructs showed cytokine release in response to blasts (Fig. 2G). Notably, functional assays highlighted a wide range of functional avidity, with six TCRs (Pt#2 WT1#2, Pt#2 WT1#2, Pt#3 WT1#3, Pt#11 WT1#2, and PT#10 hTERT#1to hTERT#4) mediating fast, specific and efficient killing of target AML blasts (fig. S17). Overall, these evidences indicate that patients' TAA-specific TCRs do not trigger responses when expressed by hypofunctional T cells but specifically recognize tumor cells presenting the target peptide in the appropriate HLA restriction when expressed by healthy T cells.

Exhaustion can be harnessed to isolate tumor-specific TCRs

We next investigated whether the T cell fraction coexpressing multiple IRs could represent a target population to isolate tumor-specific TCRs, as underlined in other cancer settings (*40*–*43*). For this purpose, T cells from three patients with AML (Pt#13to Pt#15) were harvested from the bone marrow at the time of relapse, when IR expression was the highest (*10*) and comparable between peripheral blood and bone marrow (fig. S18A). T cells were sorted into a fraction positive for multiple IRs (IR$^+$) and into a control group negative for all IRs (IR$^-$; fig. S18B). To maximize the quality of T cell stimulation and possibly revert T cell exhaustion also in the IR$^+$ T cell fraction, both T cell subpopulations were then serially stimulated with autologous blasts forced to mature into leukemic–antigen-presenting cells (L-APCs), expressing costimulatory molecules and the blast ligandome (*44*) (Fig. 3A). Both T cell fractions expanded in culture (fig. S19A), but IR$^+$ cells were more efficiently activated and exerted increased specific lysis of autologous blasts than IR$^-$ cells (Fig. 3B and fig. S19, B and C). The IR$^-$ and IR$^+$ TCR clonality was then assessed for all three patients. Despite a comparable baseline, at the end of L-APC stimulations the IR$^+$ fraction was enriched for a dominant TCR clone, present at low frequency ex vivo (Fig. 3C). We next reconstructed the dominant IR$^+$ TCRs and engineered them into previously TCR-KO T cells. In all instances, engineered T cells efficiently lysed autologous leukemic blasts (Fig. 3D) while activating (Fig. 3E), degranulating (Fig. 3F), and releasing cytokines (Fig. 3G) in the presence of target cells. These results underline how exhausted T cells at relapse are preferentially enriched in tumor specificities, how exhaustion can be reverted by a proper stimulation, and how it can be harnessed to isolate tumor-specific TCRs.

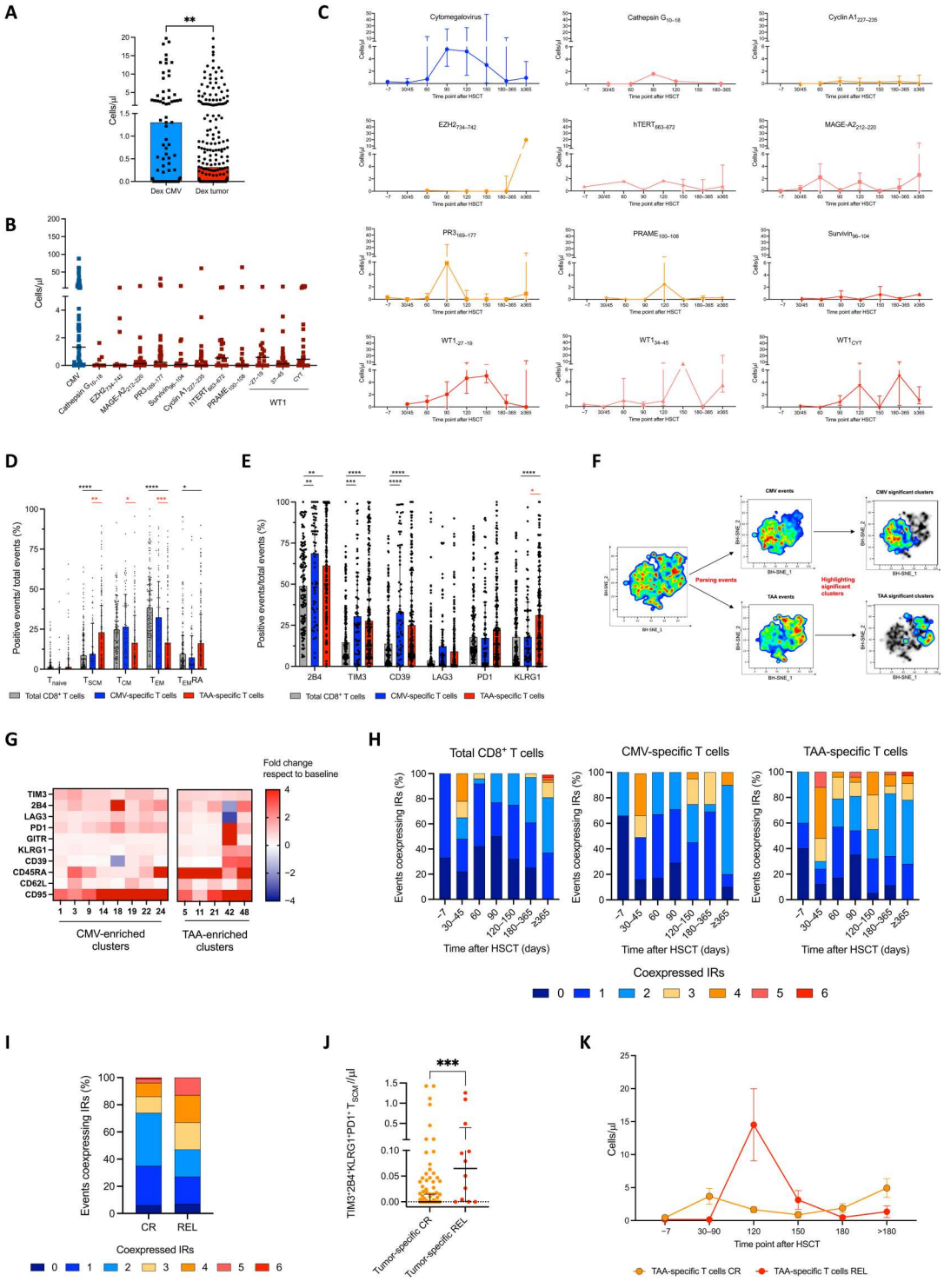

Fig. 1. TAA-specific T cells accumulate exhausted T_{SCM} cells and contract before relapse. Total circulating CD8$^+$, TAA-specific and CMV-specific T cells were evaluated in $N = 39$ transplanted patients at sequential time points. (**A** to **C**) Number of circulating CMV- and TAA-specific T cells, in all time points (A), parsed according to antigen specificity (B) and to the time point after allo-HSCT (C); median and interquartile ranges. Mann-Whitney test (A). (**D**) Memory phenotype on total CD8$^+$, CMV-specific, and TAA-specific T cells after allo-HSCT. Unpaired multiple Student's *t* tests. Median and interquartile ranges. (**E**) Frequency of IRs expression on total CD8$^+$, CMV-specific, and TAA-specific T cells. Unpaired multiple Student's *t* tests. Median and interquartile ranges. (**F** and **G**) TAA- and CMV-specific events were analyzed with cytoChain. (F) Barnes-Hut Stochastic Neighbor Embedding (BH-SNE) biaxial plot of all events (left), then divided into CMV- and TAA-specific events (mid). Areas significantly enriched with either CMV- or TAA-specific events were highlighted (right). (G) Fold change with respect to dataset baseline, in each cluster significantly enriched for either CMV- or TAA-specific events. (**H**) Frequency of IRs coexpression on total CD8$^+$, CMV-specific, and TAA-specific T cells. (**I**) IRs coexpression in TAA-specific T cells, in patients achieving long-term complete remission (CR) or experiencing relapse (REL). (**J**) Circulating exhausted T_{SCM}, parsed according to long-term disease status. Median and interquartile ranges. Mann-Whitney test. (**K**) Circulating TAA-specific T cells in patients with CR and REL. Two-way analysis of variance (ANOVA). Mean and SEM. T_{Na}, naïve T cells (CD45RA$^+$CD62L$^+$CD95$^-$); T_{SCM}, stem cell memory T cells (CD45RA$^+$CD62L$^+$CD95$^+$); T_{CM}, central memory T cells (CD45RA^{--}CD62L$^+$); T_{EM}, effector memory T cells (CD45RA$^-$CD62L$^-$); T_{EM}RA, terminal effector T cells (CD45RA$^+$CD62L$^-$). Dex CMV, CMV-specific T cells measured with dextramers. Dex tumor, TAA-specific T cells measured with dextramers. *$P < 0.05$; **$P < 0.01$; ***$P < 0.001$; ****$P < 0.0001$.

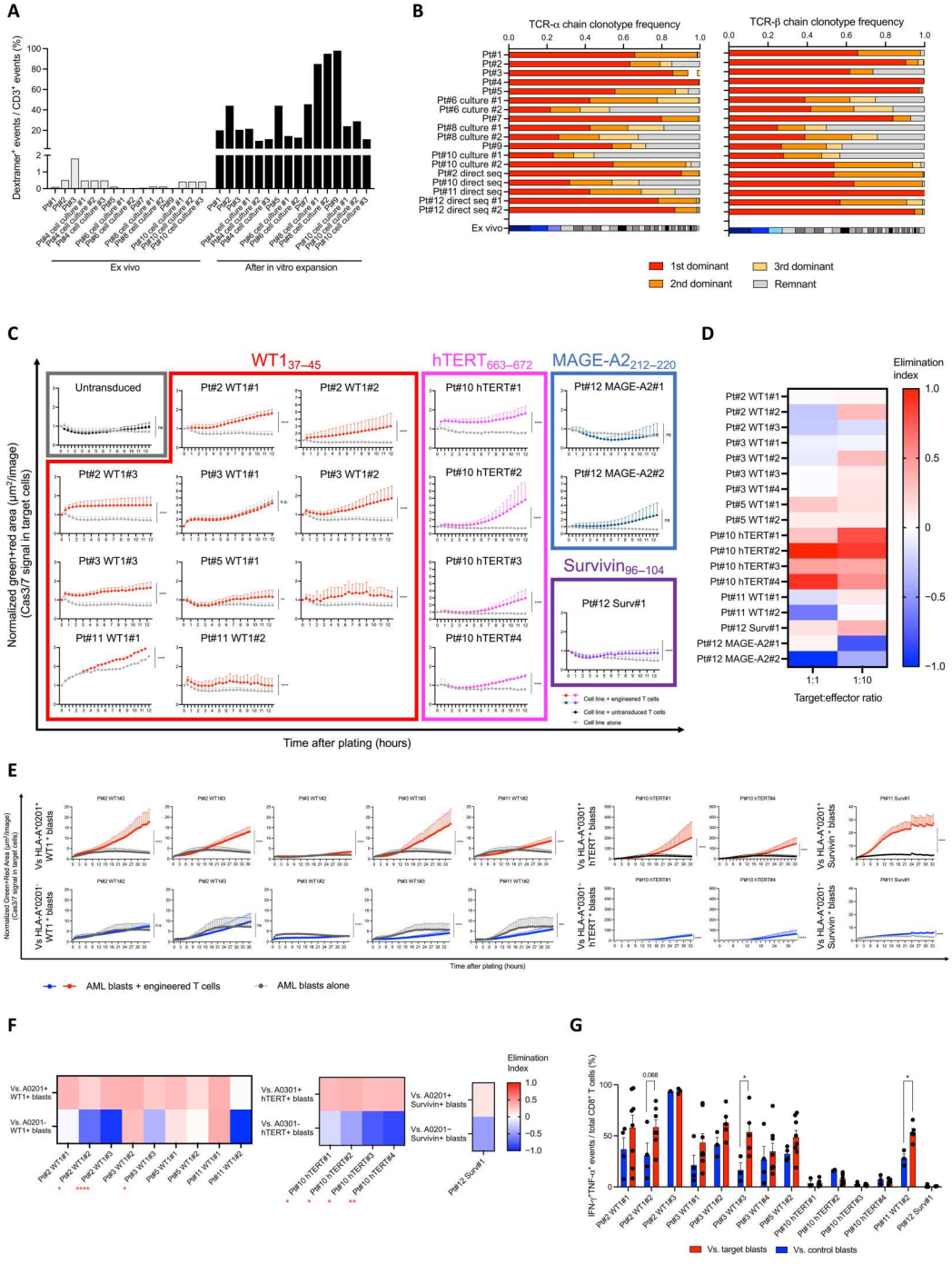

Fig. 2. Functional TAA-specific TCRs can be isolated from patients' peripheral blood. TAA-specific T cells were isolated, expanded, and then tested in vitro. (**A**) Dextramer$^+$ events ex vivo (gray bars) and after in vitro sorting and expansion (black); $N = 16$ cell cultures, $N = 10$ patients. (**B**) CDR3-α (left) and CDR3-β (right) cell culture sequences. The ex vivo clonality is reported at the bottom. (**C** to **G**) The dominant TCRs from (B) were engineered into donor T cells and then tested in vitro. (C) Edited T cells from $N = 4$ healthy donors were cocultured with peptide-pulsed T cell lines (HLA-A*0201-restricted $WT1_{37–45}$, $MAGE\text{-}A2_{212–220}$ and $survivin_{96–104}$, HLA-A*0301-restricted $hTERT_{663–672}$). The normalized Green+Red area representing the amount of target cells undergoing apoptosis (caspase 3/7 activation) overtime upon coculture with T lymphocytes is reported. (D) Edited T cells were cocultured with T cell lines pulsed either with the appropriate peptide or with an unrelated peptide ($N = 6$ experiments). The elimination index after 3 days coculture is reported [1 − (alive target cells pulsed with the target peptide and cultured with edited T cells/alive target cells pulsed with an unrelated peptide and cultured with edited T cells)]. An elimination index equal to 1 indicates total killing of target cells. (**E** to **G**) WT1-, survivin-, and hTERT-redirected engineered T cells were challenged with WT1$^+$, hTERT$^+$, or survivin$^+$ primary AML blasts expressing (target blasts, $n = 3$ per specificity) or not expressing (control blasts, $n = 3$) the appropriate HLA-restriction element. The normalized Green+Red area after coculture (E), the elimination index after 1 day of coculture (F) and the percentage of INF-γ and tumor necrosis factor–α–producing CD8$^+$ T cells are reported (G). Two-way ANOVA was used to compare curves. Multiple unpaired Student's t tests were used to compare groups in (F) and (G). *$P < 0.05$; **$P < 0.01$; ****$P < 0.0001$. The mean and the SEM are shown in (C), (E), and (G).

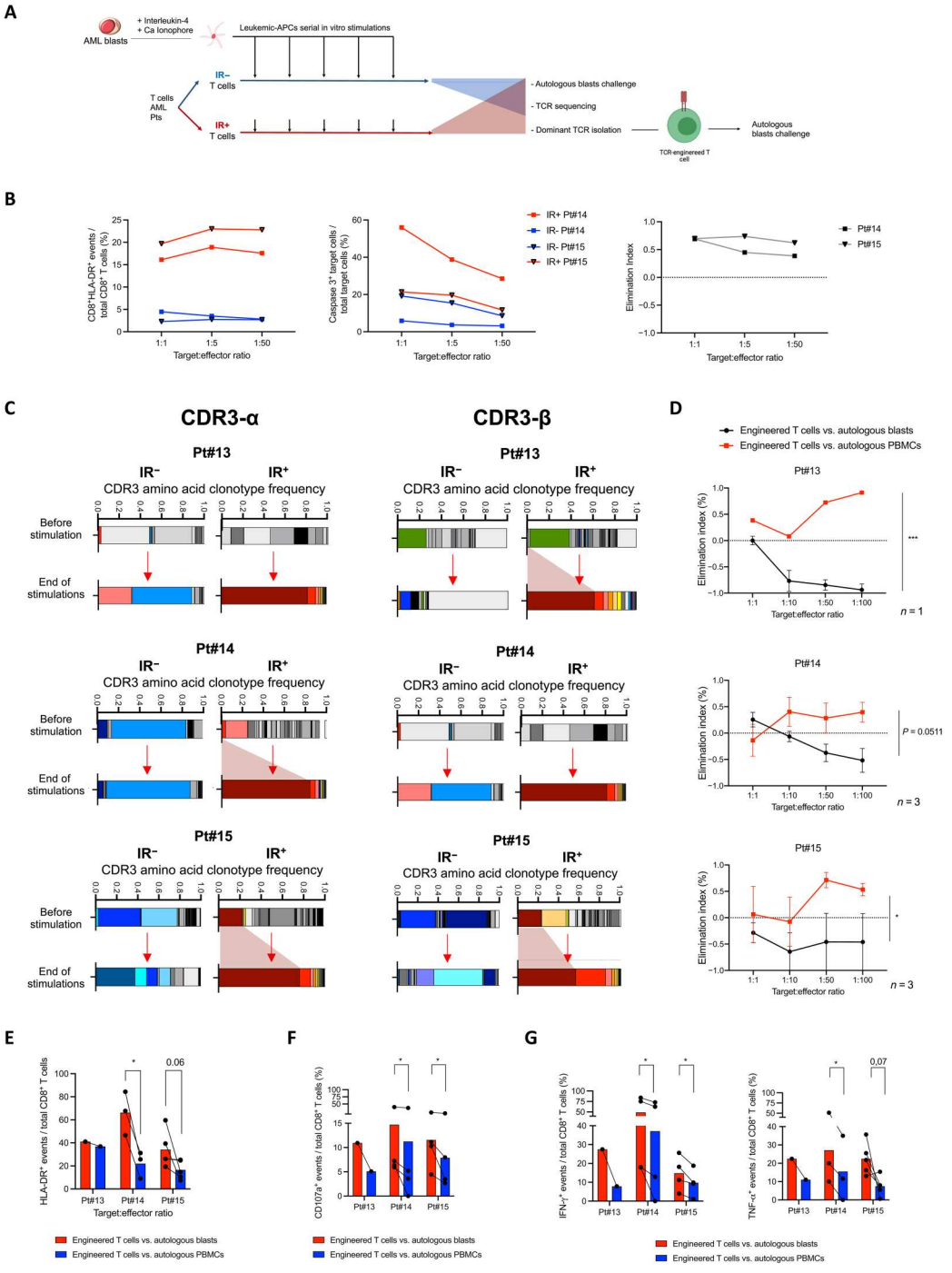

Fig. 3. The exhaustion signature can be exploited to isolate tumor-specific TCRs. Bone-marrow infiltrating T cells from Pt#13-14-15 patients at the moment of relapse were sorted into a fraction not expressing (IR^-) and a fraction expressing (IR^+) multiple IRs and then expanded in vitro by means of leukemic-antigen presenting cells (L-APCs). (**A**) Schematics of the in vitro experimental protocol. (**B**) After sequential L-APC stimulations, the IR^+ (red) and IR^- (blue) fractions from Pt#14 and Pt#15 were challenged with autologous leukemic blasts. The induction of HLA-DR on $CD8^+$ edited T cells (left), expression of activated caspase 3 on target blasts (mid), and the elimination index (right) are reported. The elimination index was calculated according to the formula [1 − (number of alive blasts cultured with IR^+ T cells/number of blasts cultured with IR^- T cells)]. (**C**) CDR3 α-(left) and β-chain (right) clonotype frequency in the IR^+ and IR^- fractions, before and after sequential L-APCs stimulation, for all the three patients tested. The expanding dominant IR^+ clone is highlighted in red. (**D** to **G**) In each patient, the dominant IR^+ TCR identified at the end of the stimulation cultures was reconstructed and engineered into T cells derived from $n = 1$ (Pt#13) and $n = 3$ (Pt#14-15) different healthy donors. Edited T cells were then challenged with either autologous leukemic blasts or autologous healthy hematopoietic cells. The elimination index (D), the activation (E), degranulation (F), and cytokine production (G) abilities of engineered T cells are reported. The elimination index was calculated using the formula [1 − (number of alive target cells cocultured with engineered T cells/number of alive target cells cocultured alone)]. Two-way ANOVA was used to compare curves in (D), paired multiple Student's *t* tests were used to compare groups in (E) to (G). The mean and the SEM are shown in (D) to (G). $*P < 0.05$; $***P < 0.001$.

Trogocytosis allows the characterization of orphan TCRs

To identify the HLA restriction and peptide specificity of the IR^+ TCRs, we harnessed the mechanism of trogocytosis and the Ligandome-on-chip technology (PeptiChip) (*32*). Trogocytosis is a phenomenon of intracellular cell membrane exchange (*31*) where T cells can translocate part of their immunological synapse, such as the TCR/CD3 complex, on target cells (*45*, *46*). Because trogocytosis has been exploited to identify the specificity of TCRs via cDNA library screening (*47*), we investigated whether this strategy could be adapted to deorphanize leukemia-specific TCRs expressed by engineered T cells. To set up the protocol, NY-ESO TCR-edited T cells (*17*) were cocultured with a mix of target U266 ($NY\text{-}ESO^+$ $HLA\text{-}A^*0201^+$) and MM1s ($NY\text{-}ESO^+$ $HLA\text{-}A^*0201^-$) cell lines. We observed that a fraction of U266 but not of MM1s cells acquired CD3 and the NY-ESO TCR, in a time-dependent manner (fig. S20, A to C). We observed no trogocytosis spillover to bystander MM1s cells and the preferential unidirectionality of the exchanges, as NY-ESO TCR-edited T cells, derived from an $HLA\text{-}A^*0201^-$ donor, did not acquire HLA-A*0201 molecules from the U266 cell line (fig.

S20D). We next tested patients' samples, and we observed that a limited but detectable fraction of blasts acquired the CD3 surface marker in a target:effector-dependent manner when cocultured with T cells engineered with the orphan TCRs derived from Pt#13 to Pt#15 and previously tested in Fig. 3 (Fig. 4, A and B). We then devised an experimental pipeline to deorphanize Pt#14 and Pt#15 TCRs by taking advantage of such phenomenon. Edited T cells expressing Pt#14 or Pt#15 orphan TCRs were first cocultured with autologous blasts, and then blasts were sorted into two fractions, either experiencing (i.e., $CD3^+$ blasts) or not experiencing ($CD3^-$ blasts) trogocytosis. Next, both fractions and the total blast population underwent ligandome analysis through the PeptiChip platform (Fig. 4C). We isolated $N = 56$ (Pt#14) and $n = 30$ (Pt#15) 8- to 11-mer peptides in the $CD3^+$ fraction by mass

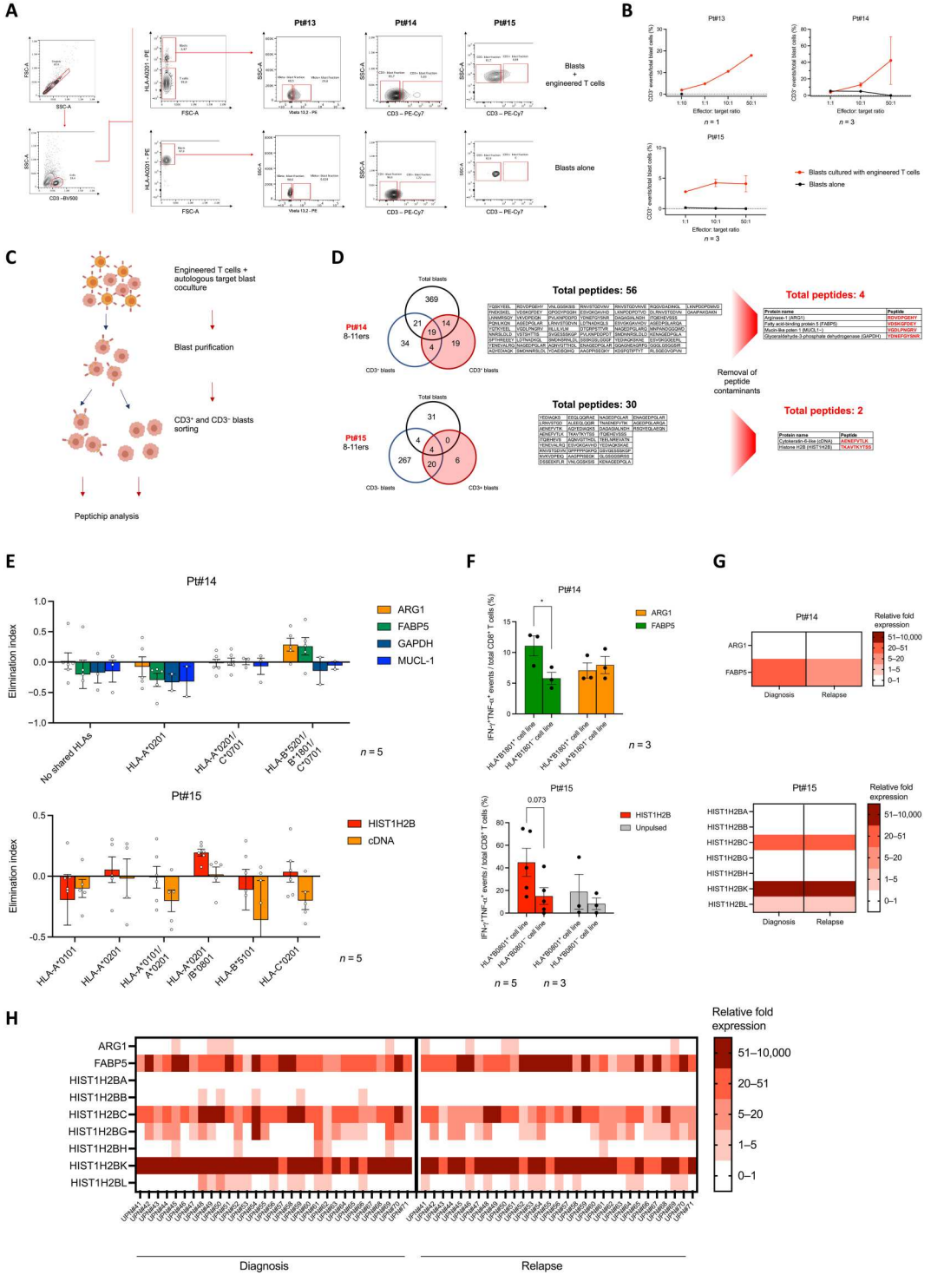

Fig. 4. PeptiChip and trogocytosis allow to deorphanize tumor-specific T-Cell Receptors. The trogocytosis effect was quantified in T cells engineered with the orphan TCRs of Fig. 3 and harnessed to perform ligandome analysis (PeptiChip). (**A** and **B**) Representative gates (A) and quantification (B) of the trogocytosis effect, defined as the percentage of blasts acquiring the CD3 T cell marker, in blast cultured with T cells engineered with Pt#13 to Pt#15 TCRs, at different effector:target ratios. (**C**) Experimental layout for the application of trogocytosis and PeptiChip for antigen discovery. (**D**) Number of 8- to 11-mers retrieved after ligandome analysis of total, $CD3^+$, and $CD3^-$ blast fractions cocultured with T cells engineered with either Pt#14 or Pt#15 TCRs, before (left) and after (right) quality control. The relevant epitopes further studied in the following panels are highlighted in red. (**E** and **F**) T cells derived from $n = 5$ different healthy donors and engineered with Pt#13 and Pt#14 TCRs were challenged in vitro with EBV-immortalized B cell lines sharing one or more HLA with the patients and pulsed with the isolated peptides. The elimination index (E) and the number of INF-γ^+TFN-α^+ $CD8^+$ T cells (F) is reported. The elimination index was calculated using the formula [1 − (number of alive peptide-pulsed target cells cocultured with engineered T cells/number of alive non peptide-pulsed target cells cocultured with engineered T cells)]. (**G** and **H**) The expression of fatty acid–binding protein 5 (FAPB5) and histone 2B (H2B) isoforms (HIST1H2BA-B-C-G-H-K-L) were quantified in Pt#14 and Pt#15, respectively (G), and in a cohort of $N = 32$ matched diagnosis/relapse blast samples pairs (H). The mean and the SEM are shown in (B), (E), and (F). *$P < 0.05$; **$P < 0.01$; ***$P < 0.001$; ****$P < 0.0001$.

spectrometry and, after removing peptides derived from protein contaminants, 4 peptides for Pt#14 and 2 peptides for Pt#15 were identified as putative cancer-associated antigen hits (Fig. 4D). Subsequently, T cell engineered with the orphan TCRs were challenged with Epstein-Barr Virus (EBV)-immortalized B cell lines expressing one or more of the patients' HLAs (fig. S20E) and pulsed with the chosen peptides. Killing (Fig. 4E) and cytokine release (Fig. 4F) assays identified an epitope derived from the fatty acid–binding protein 5 (FABP5) (*48*, *49*), mounted on HLA-B*1801, as Pt#14 TCR target, while Pt#15 engineered T cells recognized a peptide belonging to histone H2B isoforms presented by HLA-B*0801$^+$. Noticeably, FABP5 and different H2B isoforms were found to be overexpressed in Pt#14 and Pt#15, respectively, both at diagnosis and at relapse (Fig. 4G). Gene expression analysis of public datasets (*50*) underlined that FABP5 is particularly expressed by AML blasts at a greater level than healthy bone marrow cells (fig. S20F), while the analysis of 32 paired diagnosis/relapse blast samples showed a widespread overexpression of both FABP5 and H2B RNA in cancer cells (Fig. 4H). Overall, these data present a pipeline for the characterization of orphan TCRs and proved that the IR$^+$ T cell fraction is a source of tumor-specific TCRs recognizing broadly expressed AML antigens.

DISCUSSION

In the present work, we described the frequency, composition, and functional status of tumor-specific T cells in vivo and present strategies to isolate tumor-directed TCRs. Thanks to the application of an optimized staining protocol and of the cytoChain platform, we showed that T cells against several overexpressed TAA epitopes restricted for common HLAs circulate in the majority (90%) of patients early after allo-HSCT and persist long-term. TAA-specific cells are preferentially T_{SCM}/T_{EM}RA cells, suggesting priming and differentiation upon encounter with leukemic cells (*51*), and express multiple IRs, with remarkable interpatient variability on the type of IR expressed. TAA-specific T_{SCM} cells expressing multiple IRs and no activation markers enriched after transplant, preferentially in patients who subsequently relapsed (REL), and represented a consistent fraction of total TAA-specific T_{SCM} lymphocytes. Such exhausted and thus dysfunctional signature may sign the progressive failure of immune surveillance, marked by the depletion of healthy functional progenitors that can supply short-lived effectors. In REL patients, we observed a marked coexpression of IRs and a reduced number of circulating tumor-specific cells, independently of the targeted TAA antigen and despite TAA expression on blasts was unchanged. These results are suggestive of an erosion of the TAA-specific T cell pool mediated by exhaustion, impinging the long-term maintenance of tumor-reactive cells and thus potentially contributing to disease immune escape. These results also underline that although the type of IR expressed differ slightly among patients, the T cell signature converges toward IR coexpression.

We next challenged exhaustion to isolate TAA-specific TCRs. In vitro polyclonal activation enabled TAA-specific T cell expansion and TCR isolation but did not empower cytolytic functions, indicating a stepwise loss of function typical of exhausted T cells (*52*). Notably, 14 of the 18 TCRs were isolated from patients with CR, suggesting that the deeper exhaustion state observed in patients with REL may limit the recovery of TAA-specific TCRs, and possibly reflecting inefficient GvL. When the isolated TAA-TCRs were expressed on healthy T cells, specific in vitro killing was observed for most of the hTERT, survivin, and WT1 TCR-edited T cells. The evidence that not all the TCR recovered by dextramers showed the same functionality when tested, advocates for an in vitro validation after dextramer-based TCR hunting. With this approach, we found potentially clinically relevant TCRs for blood malignancies, and we underlined how TCR isolation is efficient in those patients and those time points in which TAA-specific cells are circulating.

The evidence that tumor-specific T cells are exhausted and express several IRs has been first reported for solid tumors and has been exploited to ameliorate TILs retrieval (*41*), to promote cytotoxic T lymphocytes–based therapy (*53*) and to isolate TCRs of known specificity (*41*, *54*). Here, we propose to harness the IR signature to isolate tumor-specific TCRs against untyped tumor antigens. First, we showed how both proliferation and cytolytic functions of exhausted T cells can be recovered by serial stimulations with L-APCs, while we previously failed to recover cytolytic functions with dextramer screening, suggesting that a more diverse array of costimuli is required to counteract from exhaustion. Second, we demonstrated that T cell clones recognizing AML blasts, but not healthy blood precursors, can be expanded from patients at relapse. Third, we validated the use of trogocytosis and ligandome-on-chip analysis to identify the target peptide and the HLA restriction of orphan TCRs. Thanks to this approach, we added to our portfolio additional highly functional TCRs against previously untyped relevant TAAs, widely and consistently expressed by leukemic blasts at diagnosis and relapse. The orphan TCRs recognized TAAs rather than neoantigens, a result possibly reflecting the limited number of neoantigens in AML. The efficacy of the proposed experimental protocol and the broad expression of the antigens targeted by the isolated TCRs in different patients could potentially widen the applicability of our approach to low mutational burden cancers, for which the number of TCRs to be used for T cell engineering is limited.

Overall, these results contribute to shed light on the longitudinal landscape of TAA-specific T cells after transplant and propose a way to harness such knowledge to isolate functional, tumor-specific TCRs for ACT. Both these TCRs and these approaches could be translated in different tumor contexts and have the potential to unveil previously unknown TCRs and antigens relevant for tumor immunology.

MATERIALS AND METHODS

Human biological sample handling

All samples were collected under written informed consent in agreement with the Declaration of Helsinki, previous approval by the Institutional Ethical Committee. All data needed to evaluate the conclusions in the paper are present in the paper and/or the Supplementary Materials.

Thawing of frozen material

Peripheral blood mononuclear cell (PBMC) and bone marrow samples were retrieved from the BioBank facility at San Raffaele, thawed, and kept overnight at 37°C at a concentration of 1×10^6 cells/ml in X-vivo (Lonza) supplemented with glutamine (1%),

penicillin/streptomycin (P/S) (1%), human serum 2%, and deoxyribonuclease (Roche) (1 IU/ml), as previously reported (*10*).

Dextramer staining

PBMCs were isolated via Ficoll-Hypaque gradient centrifugation (1700 rpm, 30 min). Successively, PBMCs were incubated with ammonium-chloride-potassium solution and then washed multiple times with phosphate-buffered saline (PBS) supplemented with 2% fetal bovine serum (FBS) to eliminate erythrocytes and platelets. Samples were stained with a viability dye for 15 min (Zombie dyes, Biolegend), according to the manufacturer′s instruction, and then washed with PBS supplemented with 1% FBS and centrifuged (1500 rpm, 5 min). Cells then underwent surface staining in 50 μl of brilliant stain buffer (BD Biosciences) for 15 min at room temperature (RT), washed as previously described, resuspended in 50 μl of PBS supplemented with 5% FBS and 5 μM of the tyrosine kinase inhibitor dasatinib (*34*) (Axon Medchem, VA), and incubated 15 min at 37°C. The dextramer (Immudex) mix was then added, and samples were incubated on ice for 30 min before a last washing step. Within 30 min from staining, samples were acquired at the institutional BD LSRFortessa or BD Symphony instrumentations while kept on ice. The dextramers and the antibody-associated fluorochromes used are listed in tables S1 and S2, respectively. During data analysis by FlowJo software version 10 (BD), each sample has been considered positive for dextramer staining when (i) at least 10 events fell in the $CD3^+CD8^+dextramer^+$ gate, (ii) at least 0.01% of the total T cell population fell in the $CD3^+CD8^+dextramer^+$gate, and (iii) the $CD3^+CD8^+dextramer^+$gate counted at least double the events than the $CD3^+CD4^+dextramer^+$ control gate. When a specific dextramer proved negative in two consecutive sampling from the same patient, such dextramer was not further tested in that specific patient.

High-dimensional analysis

$CD3^+CD8^+$ alive events were processed by the cytoChain platform, using a previously published pipeline (*36*). Each sample was optimized and concatenated, and memory and exhaustion markers were used to drive Barnes-Hut Stochastic Neighbor Embedding (BH-SNE) dimensionality reduction and FlowSOM clustering. The recovered complex multiparametric T cell signatures were then traced back into all samples.

In vitro coculture assays

A total of 100,000 effector T cells per condition were resuspended in X-vivo supplemented with 5% FBS, 1% P/S, and 1% glutamine. Target cells were added, at target:effector ratios between 1:1 and 1:100, according to the experimental layout. In the experiments using peptide-pulsed tumor cell lines, target cells were incubated overnight with the appropriate peptide (1 μg/ml) in RPMI (Euroclone) supplemented with 5% FBS, 1% P/S, and 1% glutamine, before plating them with effectors. For evaluating cytokine release and caspase 3 induction on target cells, plates were kept in culture for 6 hours at 37°C and 5% CO2. After incubation, cells were first stained with surface molecules (15 min at RT), then fixed (FoxP3 Fix/Perm buffer (Biolegend), 20 min), and permeabilized [FoxP3 Perm buffer (Biolegend, 20 min)], according to the manufacturer′s instructions. Samples were then stained for either intracellular caspase 3 (staining 1 hour in ice) or cytokines (staining 15 min at RT; table S2). For killing assays, cells were plated and kept at 37°C and 5% CO2 after the addition of anti-CD28 monoclonal antibody (1 μg/ml; BD Biosciences) for 72 hours in case of cocultures with cell lines, and for 24 hours for cocultures with primary AML blasts. After incubation, cells were stained with the appropriate fluorochromes (15 min at RT) and then washed. Viable target cells were counted using counting beads (flow-count fluorospheres, Beckman Coulter), according to manufacturer′s instructions. Elimination index was calculated according to the formula: [1 − (number of living target cells in culture with effector T cells/number of living target cells in control culture)]. Samples were acquired at the institutional BD CANTO or CytoFLEX (ThermoFisher) flow cytometers. Data were analyzed by FlowJo software version 10 (BD). The list of each fluorochrome-conjugated monoclonal antibody is available in table S2.

Live-cell imaging assays

Target cells were plated for coculture assays as described above. Target cells were labeled with Incucyte NucLight Rapid Red Reagent (Sartorius) according to the manufacturer′s instructions and then resuspended in X-vivo supplemented with 5% FBS, 1% P/S, and 1% glutamine, anti-CD28 monoclonal antibody (1 μg/ml) and Incucyte caspase-3/7 Green Apoptosis Assay Reagent (Sartorius). Effector T cells were then added (100,000 cells/well). The plate was analyzed at the institutional Incucyte incubator cell imager using the built-in analytical software.

TCR reconstruction and lentiviral packaging

Sequencing of the TCR α and β chains was performed on RNA by using a modified RACE PCR protocol, independently of multiplex PCRs. Samples were sequenced using the MiSeq platform (Illumina) and raw reads were sorted according to the individual barcode combination used for each specimen. Analysis of the TCR clonotypes was carried out using the MiXCR software. The identified α and β TCR chain sequences were cysteine modified, codon-optimized, synthesized (Twist Bioscience) and then inserted into plasmid vectors under a bidirectional promoter (*55*). The β chain was cloned in sense orientation under the human phosphoglycerate kinase (PGK) promoter, whereas the α chain was cloned in antisense orientation under the control of the human minimal CMV promoter (mhCMV). Plasmids were packaged into lentiviral vectors (LVs) as integrase-competent third generation constructs pseudo-typed by the vesicular stomatitis virus (VSV) envelope. The TCR was transferred into T cells using the prepared LVs into TCR-KO T cells.

Dextramer-based T cell sorting and expansion

Cells were stained with a specific dextramer as previously described and then separated by means of magnetic column sorting (Miltenyi), using either anti-phychoerythrin (anti-PE) or anti-allophycocyanin (anti-APC) magnetic beads. The sorted positive fraction was then plated in a 96-well plate previously coated with anti-CD3 (BD Biosciences, 1 μg/ml) and anti-CD28 (BD Biosciences, 2 μg/ml) mAb. Cells were supplemented with complete X-vivo +IL-7 (5 ng/ml, PeproTech) + IL-15 (5 ng/ml, PeproTech) and medium and cytokines were replaced every 2 to 3 days.

IR-based T cell sorting and expansion

T cells harvested from frozen bone marrow samples of patients who underwent allo-HSCT were separated via fluorescence-activated cell

sorting into two fractions, one expressing no IRs (IR^-) and the other coexpressing multiple IRs (IR^+). Cells were then resuspended in complete X-vivo and subsequently stimulated using autologous L-APCs every 2 weeks until expansion halted. Autologous blasts were forced to differentiate into L-APCs via a 2-day culture in complete X-vivo supplemented with IL-4 (250 IU/ml) and Calcimycin (calcium ionophore, 375 ng/ml, Sigma-Aldrich) (*44*).

PeptiChip Immunoafinity purification and mass spectrometry analysis of HLA-I peptides

HLA class I peptides were immunoaffinity purified and prepared for mass spectrometry analysis as described (*32*). Briefly, snap-frozen cell pellet was resuspended in lysis buffer and the lysate cleared by centrifugation. Next, HLA-I complexes were immunoaffinity purified from the cleared lysate with anti-human HLA-A, HLA-B, and HLA-C biotin-streptavidin bound to the micropillars of the biotinylated thiol-ene chip. Then, the HLA molecules were eluted at RT by adding acetic acid 7% (A113, Thermo Fisher Scientific, Leicestershire, UK) in 50% MetOH (10402824 Thermo Fisher Scientific, Leicestershire, UK). Eluted HLA peptides and the subunits of the HLA complexes were desalted according to a protocol previously described (*56*). Last, the samples were dried using vacuum centrifugation (Eppendorf). Approximately 20,000 cells per sample were used in PeptiChip assay analysis. Liquid chromatography–mass spectrometry (LC-MS) immunopeptidomics was performed as described (*57*). Briefly, each dry sample was dissolved in 10 µl of LC-MS solvent A (0.1% formic acid) by dispensing/aspirating 20 times with the micropipette. The nanoElute LC system (Bruker, Bremen, Germany) injected and loaded 10 µl of the sample directly onto the analytical column (Aurora C18, 25 cm long, 75-µm inside diameter, 1.6-µm bead size, Ionopticks, Melbourne, Australia) constantly kept at 50°C by a heating oven (PRSO- V2 oven, Sonation, Biberach, Germany). After washing and loading the sample at a constant pressure of 800 bar, the LC system started a 30-min gradient from 0 to 32% solvent B (acetonitrile, 0.1% formic acid), followed by an increase to 95% B in 5 min, and lastly a wash of 10 min at 95% B, all at a flow rate of 300 nl/min. Online LC-MS was performed using a Tims TOF Pro mass spectrometer (Bruker) with the CaptiveSpray source, capillary voltage 1500 V, dry gas flow of 3 liters/min, dry gas temperature at 180° C. MS data reduction was enabled. Mass spectra peak detection maximum intensity was set to 10. Mobilogram peak detection intensity threshold was set to 5000. Mass range was 300 to 1100 mass/charge ratio (m/z), and mobility range was 0.6 to 1.30 V·s/cm^2. Tandem MS (MS/MS) was used with three PASEF (parallel accumulation − serial fragmentation) scans (300 ms each) per cycle with a target intensity of 20 000 and intensity threshold of 1000, considering charge states 0 to 5. Active exclusion was used with release after 0.4 min, reconsidering precursor if the current intensity is greater than fourfold the previous intensity, and a mass width of 0.015 m/z and a 1/k0 width of 0.015 V·s/cm^2. Isolation width was defined as 2.00 m/z for mass 700 m/z and 3.00 m/z for mass 800 m/z. Collision energy was set as 10.62 eV for 1/k0 0.60 V·s/cm^2 and 51.46 eV for 1/k0 1.30 V·s/cm^2. Precursor ions were selected using 1 MS repetition and a cycle overlap of 1 with the default intensities/repetitions schedule.

Immunopeptidomics database search

All MS/MS spectra were searched by PEAKS Studio X+ (v10.5 build 16 October 2019) using a target-decoy strategy. The database used was the Uniprot Human reference proteome database (including isoforms, 98,997 entries, downloaded from uniprot.org on 29 January 2021). A precursor mass tolerance of 20 ppm and a product mass tolerance of 0.02 Da for CID-ITMS2 were used. Settings were defined as follows: Enzyme none, digest mode unspecific, and oxidation of methionine was used as variable modification, with max three oxidations per peptide. A false discovery rate cutoff of 1% was used at the peptide level to remove MS noise. The resulted peptide hits were then filtered per peptide length and 8- to 12-mers, the most likely to bind an HLA pocket *(58)* further analyzed. To remove additional peptide contaminants, we excluded by cross-search in the Uniprot Human reference proteome database those peptides expressed by nonhematological cell lineage and likely representing contaminants (e.g., skin contaminants acquired during the sampling procedure). The mass spectrometry proteomics data have been deposited to the ProteomeXchange Consortium via the PRIDE partner repository with the dataset identifier PXD035344.

RNA sequencing of blast samples

WT1 expression was evaluated as routine clinical screening with quantitative PCRs. Gene expression levels of $N = 32$ diagnosis/relapse purified blast sample pairs were quantified as in the study of Toffalori *et al.* (*11*) by pseudo-aligning read tags to gencode v.28 transcripts (*59*) using kallisto v.0.44.0[27043002] with parameters: -t 8—single—rf-stranded -l 200 -s 20. Abundancies were then summarized to gene level using the tximport R package (*60*).

TCR gene editing

PBMC harvested from healthy donors were activated using anti-CD3/anti-CD28-coated magnetic beads (ClinExVivo CD3/CD28; Invitrogen) and maintained at a concentration of 10^6 cells/ml in complete X-vivo supplemented with IL-7 + IL-15 (5 ng/ml each). Two days after stimulation, T cells were electroporated with RNP complexes [consisting of purified Spy Cas9 nuclease (Intellia Therapeutics) (*38*)] duplexed with synthetic gRNAs) targeting the *TRAC* and the *TRBC1/2* loci simultaneously using the Lonza Nucleofector 4D Electroporation System. The day after, T cells were transduced with a LV encoding for the tumor-specific TCR of interest. At day 6 after stimulation, beads were removed from culture and between day 14 and day 21 either tested in coculture assays or frozen and subsequently used for in vivo studies.

Software used

FlowJo software v 10.0 was used for flow cytometry files manual gating and from the figures biaxial plots. Prism Prism 9.3.1 (GraphPad Software, San Diego, California, USA) was used for data rendering and statistical analysis.

Statistical analyses

Two-tailed unpaired Student's t test was used to compare two groups at a time, when data sparsity between groups was comparable and events normally distributed. Mann-Whitney test was used to compare two non-normally distributed groups. Two-way analysis of variance (ANOVA) or mixed models with Sidak's multiple comparisons tests were used to compare multiple groups and multiple

variables simultaneously. One-way ANOVA was used to compare normally distributed multiple groups, while Kruskal-Wallis tests were used to compare non-normally distributed multiple groups. The statistical methods used are detailed in each figure legend. Data are expressed as means ± SEM unless otherwise specified. Tests were performed using Prism 9.3.1 (GraphPad Software, San Diego, California, USA). P values < 0.05 were taken to indicate statistical significance unless otherwise stated.

Supplementary Materials

This PDF file includes:

Figs. S1 to S20
Tables S1 and S2

REFERENCES AND NOTES

1. M. M. Horowitz, R. P. Gale, P. M. Sondel, J. M. Goldman, J. Kersey, H.-J. Kolb, A. A. Rimm, O. Ringdén, C. Rozman, B. Speck, R. L. Truitt, F. E. Zwaan, M. M. Bortin, Graft-versus-leukemia reactions after bone marrow transplantation. *Blood* **75**, 555–562 (1990).
2. J. Styczyński, G. Tridello, L. Koster, S. Iacobelli, A. van Biezen, S. van der Werf, M. Mikulska, L. Gil, C. Cordonnier, P. Ljungman, D. Averbuch, S. Cesaro, R. de la Camara, H. Baldomero, P. Bader, G. Basak, C. Bonini, R. Duarte, C. Dufour, J. Kuball, A. Lankester, S. Montoto, A. Nagler, J. A. Snowden, N. Kröger, M. Mohty, A. Gratwohl; Infectious Diseases Working Party EBMT, Death after hematopoietic stem cell transplantation: changes over calendar year time, infections and associated factors. *Bone Marrow Transplant.* **55**, 126–136 (2020).
3. E. J. Wherry, M. Kurachi, Molecular and cellular insights into T cell exhaustion. *Nat. Rev. Immunol.* **15**, 486–499 (2015).
4. S. P. D'angelo, L. Melchiori, M. S. Merchant, D. Bernstein, J. Glod, R. Kaplan, S. Grupp, W. D. Tap, K. Chagin, G. K. Binder, S. Basu, D. E. Lowther, R. Wang, N. Bath, A. Tipping, G. Betts, I. Ramachandran, J.-M. Navenot, H. Zhang, D. K. Wells, E. Van Winkle, G. Kari, T. Trivedi, T. Holdich, L. Pandite, R. Amado, C. L. Mackall, Antitumor activity associated with prolonged persistence of adoptively transferred NY-ESO-1 ^{c259}T cells in synovial sarcoma. *Cancer Discov.* **8**, 944–957 (2018).
5. A. G. Chapuis, D. N. Egan, M. Bar, T. M. Schmitt, M. S. McAfee, K. G. Paulson, V. Voillet, R. Gottardo, G. B. Ragnarsson, M. Bleakley, C. C. Yeung, P. Muhlhauser, H. N. Nguyen, L. A. Kropp, L. Castelli, F. Wagener, D. Hunter, M. Lindberg, K. Cohen, A. Seese, M. J. McElrath, N. Duerkopp, T. A. Gooley, P. D. Greenberg, T cell receptor gene therapy targeting WT1 prevents acute myeloid leukemia relapse post-transplant. *Nat. Med.* **25**, 1064–1072 (2019).
6. D. S. Thommen, T. N. Schumacher, T cell dysfunction in cancer. *Cancer Cell* **33**, 547–562 (2018).
7. G. Oliveira, K. Stromhaug, S. Klaeger, T. Kula, D. T. Frederick, P. M. Le, J. Forman, T. Huang, S. Li, W. Zhang, Q. Xu, N. Cieri, K. R. Clauser, S. A. Shukla, D. Neuberg, S. Justesen, G. MacBeath, S. A. Carr, E. F. Fritsch, N. Hacohen, M. Sade-Feldman, K. J. Livak, G. M. Boland, P. A. Ott, D. B. Keskin, C. J. Wu, Phenotype, specificity and avidity of antitumour CD8$^+$ T cells in melanoma. *Nature* **596**, 119–125 (2021).
8. M. C. Lahman, T. M. Schmitt, K. G. Paulson, N. Vigneron, D. Buenrostro, F. D. Wagener, V. Voillet, L. Martin, R. Gottardo, J. Bielas, J. M. McElrath, D. L. Stirewalt, E. L. Pogosova-Agadjanyan, C. C. Yeung, R. H. Pierce, D. N. Egan, M. Bar, P. C. Hendrie, S. Kinsella, A. Vakil, J. Butler, M. Chaffee, J. Linton, M. S. McAfee, D. S. Hunter, M. Bleakley, A. Rongvaux, B. J. Van den Eynde, A. G. Chapuis, P. D. Greenberg, Targeting an alternate Wilms' tumor antigen 1 peptide bypasses immunoproteasome dependency. *Sci. Transl. Med.* **14**, eabg8070 (2022).
9. A. Legat, D. E. Speiser, H. Pircher, D. Zehn, S. A. Fuertes Marraco, Inhibitory receptor expression depends more dominantly on differentiation and activation than "exhaustion" of human CD8 T cells. *Front. Immunol.* **4**, 455 (2013).
10. M. Noviello, F. Manfredi, E. Ruggiero, T. Perini, G. Oliveira, F. Cortesi, P. De Simone, C. Toffalori, V. Gambacorta, R. Greco, J. Peccatori, M. Casucci, G. Casorati, P. Dellabona, M. Onozawa, T. Teshima, M. Griffioen, C. J. M. Halkes, J. H. F. Falkenburg, F. Stölzel, H. Altmann, M. Bornhäuser, M. Waterhouse, R. Zeiser, J. Finke, N. Cieri, A. Bondanza, L. Vago, F. Ciceri, C. Bonini, Bone marrow central memory and memory stem T-cell exhaustion in AML patients relapsing after HSCT. *Nat. Commun.* **10**, 1065 (2019).
11. C. Toffalori, L. Zito, V. Gambacorta, M. Riba, G. Oliveira, G. Bucci, M. Barcella, O. Spinelli, R. Greco, L. Crucitti, N. Cieri, M. Noviello, F. Manfredi, E. Montaldo, R. Ostuni, M. M. Naldini, B. Gentner, M. Waterhouse, R. Zeiser, J. Finke, M. Hanoun, D. W. Beelen, I. Gojo, L. Luznik, M. Onozawa, T. Teshima, R. Devillier, D. Blaise, C. J. M. Halkes, M. Griffioen, M. G. Carrabba, M. Bernardi, J. Peccatori, C. Barlassina, E. Stupka, D. Lazarevic, G. Tonon, A. Rambaldi, D. Cittaro, C. Bonini, K. Fleischhauer, F. Ciceri, L. Vago, Immune signature drives leukemia escape and relapse after hematopoietic cell transplantation. *Nat. Med.* **25**, 603–611 (2019).
12. T. J. A. Hutten, W. J. Norde, R. Woestenenk, R. C. Wang, F. Maas, M. Kester, J. H. F. Falkenburg, S. Berglund, L. Luznik, J. H. Jansen, N. Schaap, H. Dolstra, W. Hobo, Increased coexpression of PD-1, TIGIT, and KLRG-1 on tumor-reactive CD8$^+$ T cells during relapse after allogeneic stem cell transplantation. *Biol. Blood Marrow Transplant.* **24**, 666–677 (2018).
13. L. Gattinoni, E. Lugli, Y. Ji, Z. Pos, C. M. Paulos, M. F. Quigley, J. R. Almeida, E. Gostick, Z. Yu, C. Carpenito, E. Wang, D. C. Douek, D. A. Price, C. H. June, F. M. Marincola, M. Roederer, N. P. Restifo, A human memory T-cell subset with stem cell-like properties. *Nat. Med.* **17**, 1290–1297 (2011).
14. N. Cieri, B. Camisa, F. Cocchiarella, M. Forcato, G. Oliveira, E. Provasi, A. Bondanza, C. Bordignon, J. Peccatori, F. Ciceri, M. T. Lupo-Stanghellini, F. Mavilio, A. Mondino, S. Bicciato, A. Recchia, C. Bonini, IL-7 and IL-15 instruct the generation of human memory stem T cells from naive precursors. *Blood* **121**, 573–584 (2013).
15. B. M. Haverkos, D. Abbott, M. Hamadani, P. Armand, M. E. Flowers, R. Merryman, M. Kamdar, A. S. Kanate, A. Saad, A. Mehta, S. Ganguly, T. S. Fenske, P. Hari, R. Lowsky, L. Andritsos, M. Jagasia, A. Bashey, S. Brown, V. Bachanova, D. Stephens, S. Mineishi, R. Nakamura, Y.-B. Chen, B. R. Blazar, J. Gutman, S. M. Devine, PD-1 blockade for relapsed lymphoma post-allogeneic hematopoietic cell transplant: High response rate but frequent GVHD. *Blood* **130**, 221–228 (2017).
16. N. Köhler, D. A. Ruess, R. Kesselring, R. Zeiser, The role of immune checkpoint molecules for relapse after allogeneic hematopoietic cell transplantation. *Front. Immunol.* **12**, 634435 (2021).
17. A. P. Rapoport, E. A. Stadtmauer, G. K. Binder-Scholl, O. Goloubeva, D. T. Vogl, S. F. Lacey, A. Z. Badros, A. Garfall, B. Weiss, J. Finklestein, I. Kulikovskaya, S. K. Sinha, S. Kronsberg, M. Gupta, S. Bond, L. Melchiori, J. E. Brewer, A. D. Bennett, A. B. Gerry, N. J. Pumphrey, D. Williams, H. K. Tayton-Martin, L. Ribeiro, T. Holdich, S. Yanovich, N. Hardy, J. Yared, N. Kerr, S. Philip, S. Westphal, D. L. Siegel, B. L. Levine, B. K. Jakobsen, M. Kalos, C. H. June, NY-ESO-1-specific TCR-engineered T cells mediate sustained antigen-specific antitumor effects in myeloma. *Nat. Med.* **21**, 914–921 (2015).
18. F. T. Basheer, G. Giotopoulos, E. Meduri, H. Yun, M. Mazan, D. Sasca, P. Gallipoli, L. Marando, M. Gozdecka, O. Sheppard, M. Dudek, L. Bullinger, H. Dohner, R. Dillon, S. Freeman, O. Ottman, A. Burnett, N. Russell, E. Papaemmanuil, R. Hills, P. Campbell, G. S. Vassiliou, B. J. P. Huntly, Contrasting requirements during disease evolution identify EZH2 as a therapeutic target in AML. *J. Exp. Med.* **216**, 966–981 (2019).
19. O. Goodyear, A. Agathanggelou, I. Novitzky-Basso, S. Siddique, T. McSkeane, G. Ryan, P. Vyas, J. Cavenagh, T. Stankovic, P. Moss, C. Craddock, Induction of a CD8+ T-cell response to the MAGE cancer testis antigen by combined treatment with azacitidine and sodium valproate in patients with acute myeloid leukemia and myelodysplasia. *Blood* **116**, 1908–1918 (2010).
20. J. Arai, M. Yasukawa, H. Ohminami, M. Kakimoto, A. Hasegawa, S. Fujita, Identification of human telomerase reverse transcriptase-derived peptides that induce HLA-A24-restricted antileukemia cytotoxic T lymphocytes. *Blood* **97**, 2903–2907 (2001).
21. C. Arber, X. Feng, H. Abhyankar, E. Romero, M.-F. Wu, H. E. Heslop, P. Barth, G. Dotti, B. Savoldo, Survivin-specific T cell receptor targets tumor but not T cells. *J. Clin. Invest.* **125**, 157–168 (2015).
22. J. J. Molldrem, E. Clave, Y. Z. Jiang, D. Mavroudis, A. Raptis, N. Hensel, V. Agarwala, A. J. Barrett, Cytotoxic T lymphocytes specific for a nonpolymorphic proteinase 3 peptide preferentially inhibit chronic myeloid leukemia colony-forming units. *Blood* **90**, 2529–2534 (1997).
23. C. Quintarelli, G. Dotti, B. De Angelis, V. Hoyos, M. Mims, L. Luciano, H. E. Heslop, C. M. Rooney, F. Pane, B. Savoldo, Cytotoxic T lymphocytes directed to the preferentially expressed antigen of melanoma (PRAME) target chronic myeloid leukemia. *Blood* **112**, 1876–1885 (2008).
24. K. Rezvani, A. S. M. Yong, B. N. Savani, S. Mielke, K. Keyvanfar, E. Gostick, D. A. Price, D. C. Douek, A. J. Barrett, Graft-versus-leukemia effects associated with detectable Wilms tumor-1 specific T lymphocytes after allogeneic stem-cell transplantation for acute lymphoblastic leukemia. *Blood* **110**, 1924–1932 (2007).
25. M. Kapp, S. Stevanović, K. Fick, S. M. Tan, J. Loeffler, A. Opitz, T. Tonn, G. Stuhler, H. Einsele, G. U. Grigoleit, CD8$^+$ T-cell responses to tumor-associated antigens correlate with superior relapse-free survival after allo-SCT. *Bone Marrow Transplant.* **43**, 399–410 (2009).
26. A. G. Chapuis, G. B. Ragnarsson, H. N. Nguyen, C. N. Chaney, J. S. Pufnock, T. M. Schmitt, N. Duerkopp, I. M. Roberts, G. L. Pogosov, W. Y. Ho, S. Ochsenreither, M. Wölf, M. Bar, J. P. Radich, C. Yee, P. D. Greenberg, M. Wölfl, M. Bar, J. P. Radich, C. Yee, P. D. Greenberg, M. Wölf, M. Bar, J. P. Radich, C. Yee, P. D. Greenberg, Transferred WT1-reactive CD8$^+$ T cells can mediate antileukemic activity and persist in post-transplant patients. *Sci. Transl. Med.* **5**, 174ra27 (2013).
27. P. D. Lulla, S. Naik, S. Vasileiou, I. Tzannou, A. Watanabe, M. Kuvalekar, S. Lulla, G. Carrum, C. A. Ramos, R. Kamble, L. Q. Hill, J. Randhawa, S. Gottschalk, R. Krance, T. Wang, M. Wu, C. Robertson, A. P. Gee, B. Chung, B. Grilley, M. K. Brenner, H. E. Heslop, J. F. Vera, A. M. Leen,

Clinical effects of administering leukemia-specific donor T cells to patients with AML/MDS after allogeneic transplant. *Blood* **137**, 2585–2597 (2021).
28. F. Manfredi, B. C. Cianciotti, A. Potenza, E. Tassi, M. Noviello, A. Biondi, F. Ciceri, C. Bonini, E. Ruggiero, TCR redirected T cells for cancer treatment: Achievements, hurdles, and goals. *Front. Immunol.* **11**, 1689 (2020).
29. B. Howie, A. M. Sherwood, A. D. Berkebile, J. Berka, R. O. Emerson, D. W. Williamson, I. Kirsch, M. Vignali, M. J. Rieder, C. S. Carlson, H. S. Robins, High-throughput pairing of T cell receptor α and β sequences. *Sci. Transl. Med.* **7**, 301ra131 (2015).
30. A. K. Bentzen, A. M. Marquard, R. Lyngaa, S. K. Saini, S. Ramskov, M. Donia, L. Such, A. J. S. Furness, N. McGranahan, R. Rosenthal, P. T. Straten, Z. Szallasi, I. M. Svane, C. Swanton, S. A. Quezada, S. N. Jakobsen, A. C. Eklund, S. R. Hadrup, Large-scale detection of antigen-specific T cells using peptide-MHC-I multimers labeled with DNA barcodes. *Nat. Biotechnol.* **34**, 1037–1045 (2016).
31. S. Zhao, L. Zhang, S. Xiang, Y. Hu, Z. Wu, J. Shen, Gnawing between cells and cells in the immune system: Friend or foe? A review of trogocytosis. *Front. Immunol.* **13**, 791006 (2022).
32. S. Feola, M. Haapala, K. Peltonen, C. Capasso, B. Martins, G. Antignani, A. Federico, V. Pietiäinen, J. Chiaro, M. Feodoroff, S. Russo, A. Rannikko, M. Fusciello, S. Koskela, J. Partanen, F. Hamdan, S. M. Tähkä, E. Ylösmäki, D. Greco, M. Grönholm, T. Kekarainen, M. Eshaghi, O. L. Gurvich, S. Ylä-Herttuala, R. M. Rui, J. Lehtiö, T. M. Sikanen, V. Cerullo, PeptiCHIP: A microfluidic platform for tumor antigen landscape identification. *ACS Nano* **15**, 15992–16010 (2021).
33. L. Wooldridge, A. Lissina, D. K. Cole, H. A. Van Den Berg, D. A. Price, A. K. Sewell, Tricks with tetramers: How to get the most from multimeric peptide–MHC. *Immunology* **126**, 147–164 (2009).
34. G. Dolton, K. Tungatt, A. Lloyd, V. Bianchi, S. M. Theaker, A. Trimby, C. J. Holland, M. Donia, A. J. Godkin, D. K. Cole, P. Thor Straten, M. Peakman, I. M. Svane, A. K. Sewell, More tricks with tetramers: A practical guide to staining T cells with peptide–MHC multimers. *Immunology* **146**, 11–22 (2015).
35. A. Cossarizza, H.-D. Chang, A. Radbruch, A. Acs, D. Adam, S. Adam-Klages, W. W. Agace, N. Aghaeepour, M. Akdis, M. Allez, L. N. Almeida, G. Alvisi, G. Anderson, I. Andrä, F. Annunziato, A. Anselmo, P. Bacher, C. T. Baldari, S. Bari, V. Barnaba, J. Barros-Martins, L. Battistini, W. Bauer, S. Baumgart, N. Baumgarth, D. Baumjohann, B. Baying, M. Bebawy, B. Becher, W. Beisker, V. Benes, R. Beyaert, A. Blanco, D. A. Boardman, C. Bogdan, J. G. Borger, G. Borsellino, P. E. Boulais, J. A. Bradford, D. Brenner, R. R. Brinkman, A. E. S. Brooks, D. H. Busch, M. Büscher, T. P. Bushnell, F. Calzetti, G. Cameron, I. Cammarata, X. Cao, S. L. Cardell, Guidelines for the use of flow cytometry and cell sorting in immunological studies (second edition). *Eur. J. Immunol.* **49**, 1457–1973 (2019). DOI:10.1002/eji.201970107.
36. F. Manfredi, D. Abbati, B. C. Cianciotti, L. Stasi, A. Potenza, E. Ruggiero, Z. Magnani, E. Carnevale, M. Doglio, M. Noviello, E. Tassi, C. Balestrieri, S. Buonanno, F. Clemente, C. De Lalla, M. P. Protti, A. Mondino, G. Casorati, P. Dellabona, C. Bonini, Flow cytometry data mining by cytoChain identifies determinants of exhaustion and stemness in TCR-engineered T cells. *Eur. J. Immunol.* **51**, 1992–2005 (2021).
37. E. Ruggiero, J. P. Nicolay, R. Fronza, A. Arens, A. Paruzynski, A. Nowrouzi, G. Ürenden, C. Lulay, S. Schneider, S. Goerdt, H. Glimm, P. H. Krammer, M. Schmidt, C. von Kalle, High-resolution analysis of the human T-cell receptor repertoire. *Nat. Commun.* **6**, 8081 (2015).
38. E. Ruggiero, E. Carnevale, A. Prodeus, Z. I. Magnani, B. Camisa, I. Merelli, C. Politano, L. Stasi, A. Potenza, B. C. Cianciotti, F. Manfredi, M. Di Bono, L. Vago, M. Tassara, S. Mastaglio, M. Ponzoni, F. Sanvito, D. Liu, I. Balwani, R. Galli, M. Genua, R. Ostuni, M. Doglio, D. O'Connell, I. Dutta, S. A. Yazinski, M. McKee, M. S. Arredouani, B. Schultes, F. Ciceri, C. Bonini, CRISPR-based gene disruption and integration of high-avidity, WT1-specific T cell receptors improve antitumor T cell function. *Sci. Transl. Med.* **14**, eabg8027 (2022).
39. C. Ottensmeier, M. Bowers, D. Hamid, T. Maishman, S. Regan, W. Wood, A. Cazaly, L. Stanton, Wilms' tumour antigen 1 Immunity via DNA fusion gene vaccination in haematological malignancies by intramuscular injection followed by intramuscular electroporation: a Phase II non-randomised clinical trial (WIN) (2016) (available at http://europepmc.org/books/NBK355745).
40. L. Baitsch, P. Baumgaertner, E. Devêvre, S. K. Raghav, A. Legat, L. Barba, S. Wieckowski, H. Bouzourene, B. Deplancke, P. Romero, N. Rufer, D. E. Speiser, Exhaustion of tumor-specific $CD8^+$ T cells in metastases from melanoma patients. *J. Clin. Invest.* **121**, 2350–2360 (2011).
41. A. Gros, P. F. Robbins, X. Yao, Y. F. Li, S. Turcotte, E. Tran, J. R. Wunderlich, A. Mixon, S. Farid, M. E. Dudley, K. Hanada, J. R. Almeida, S. Darko, D. C. Douek, J. C. Yang, S. A. Rosenberg, PD-1 identifies the patient-specific $CD8^+$ tumor-reactive repertoire infiltrating human tumors. *J. Clin. Invest.* **124**, 2246–2259 (2014).
42. J. J. Severson, H. S. Serracino, V. Mateescu, C. D. Raeburn, R. C. McIntyre, S. B. Sams, B. R. Haugen, J. D. French, PD-1^+Tim-3^+ $CD8^+$ T lymphocytes display varied degrees of functional exhaustion in patients with regionally metastatic differentiated thyroid cancer. *Cancer Immunol. Res.* **3**, 620–630 (2015).
43. M. Martinez, E. K. Moon, CAR T cells for solid tumors: New strategies for finding, infiltrating, and surviving in the tumor microenvironment. *Front. Immunol.* **10**, 128 (2019).
44. M. Casucci, S. K. Perna, L. Falcone, B. Camisa, Z. Magnani, M. Bernardi, A. Crotta, C. Tresoldi, K. Fleischhauer, M. Ponzoni, S. Gregori, F. Caligaris Cappio, F. Ciceri, C. Bordignon, A. Cignetti, A. Bondanza, C. Bonini, Graft-versus-leukemia effect of HLA-haploidentical central-memory T-cells expanded with leukemic APCs and modified with a suicide gene. *Mol. Ther.* **21**, 466–475 (2013).
45. T. He, C. Tang, Y. Liu, Z. Ye, X. Wu, Y. Wei, T. Moyana, J. Xiang, Bidirectional membrane molecule transfer between dendritic and T cells. *Biochem. Biophys. Res. Commun.* **359**, 202–208 (2007).
46. J. H. Shin, J. Jeong, S. E. Maher, H.-W. Lee, J. Lim, A. L. M. Bothwell, Colon cancer cells acquire immune regulatory molecules from tumor-infiltrating lymphocytes by trogocytosis. *Proc. Natl. Acad. Sci. U.S.A.* **118**, e2110241118 (2021).
47. G. Li, M. T. Bethune, S. Wong, A. V. Joglekar, M. T. Leonard, J. K. Wang, J. T. Kim, D. Cheng, S. Peng, J. M. Zaretsky, Y. Su, Y. Luo, J. R. Heath, A. Ribas, O. N. Witte, D. Baltimore, T cell antigen discovery via trogocytosis. *Nat. Methods* **16**, 183–190 (2019).
48. C. Jing, C. Beesley, C. S. Foster, P. S. Rudland, H. Fujii, T. Ono, H. Chen, P. H. Smith, Y. Ke, Identification of the messenger RNA for human cutaneous fatty acid-binding protein as a metastasis inducer. *Cancer Res.* **60**, 2390–2398 (2000).
49. S. Senga, N. Kobayashi, K. Kawaguchi, A. Ando, H. Fujii, Fatty acid-binding protein 5 (FABP5) promotes lipolysis of lipid droplets, de novo fatty acid (FA) synthesis and activation of nuclear factor-kappa B (NF-κB) signaling in cancer cells. *Biochim. Biophys. Acta - Mol. Cell Biol. Lipids* **1863**, 1057–1067 (2018).
50. M. Uhlen, C. Zhang, S. Lee, E. Sjöstedt, L. Fagerberg, G. Bidkhori, R. Benfeitas, M. Arif, Z. Liu, F. Edfors, K. Sanli, K. Von Feilitzen, P. Oksvold, E. Lundberg, S. Hober, P. Nilsson, J. Mattsson, J. M. Schwenk, H. Brunnström, B. Glimelius, T. Sjöblom, P.-H. Edqvist, D. Djureinovic, P. Micke, C. Lindskog, A. Mardinoglu, F. Ponten, A pathology atlas of the human cancer transcriptome. *Science* **357**, eaan2507 (2017).
51. N. Cieri, R. Greco, L. Crucitti, M. Morelli, F. Giglio, G. Levati, A. Assanelli, M. G. Carrabba, L. Bellio, R. Milani, F. Lorentino, M. T. L. Stanghellini, T. De Freitas, S. Marktel, M. Bernardi, C. Corti, L. Vago, C. Bonini, F. Ciceri, J. Peccatori, Post-transplantation Cyclophosphamide and Sirolimus after Haploidentical Hematopoietic stem cell transplantation using a Treosulfan-based Myeloablative conditioning and peripheral blood stem cells. *Biol. Blood Marrow Transplant.* **21**, 1506–1514 (2015).
52. C. U. Blank, W. N. Haining, W. Held, P. G. Hogan, A. Kallies, E. Lugli, R. C. Lynn, M. Philip, A. Rao, N. P. Restifo, A. Schietinger, T. N. Schumacher, P. L. Schwartzberg, A. H. Sharpe, D. E. Speiser, E. J. Wherry, B. A. Youngblood, D. Zehn, Defining 'T cell exhaustion'. *Nat. Rev. Immunol.* **19**, 665–674 (2019).
53. A. G. Chapuis, I. M. Roberts, J. A. Thompson, K. A. Margolin, S. Bhatia, S. M. Lee, H. L. Sloan, I. P. Lai, E. A. Farrar, F. Wagener, K. C. Shibuya, J. Cao, J. D. Wolchok, P. D. Greenberg, C. Yee, T-cell therapy using interleukin-21-primed cytotoxic T-cell lymphocytes combined with cytotoxic T-cell lymphocyte antigen-4 blockade results in long-term cell persistence and durable tumor regression. *J. Clin. Oncol.* **34**, 3787–3795 (2016).
54. A. Gros, E. Tran, M. R. Parkhurst, S. Ilyas, A. Pasetto, E. M. Groh, P. F. Robbins, R. Yossef, A. Garcia-Garijo, C. A. Fajardo, T. D. Prickett, L. Jia, J. J. Gartner, S. Ray, L. Ngo, J. R. Wunderllich, J. C. Yang, S. A. Rosenberg, Recognition of human gastrointestinal cancer neoantigens by circulating PD-1^+ lymphocytes. *J. Clin. Invest.* **129**, 4992–5004 (2019).
55. M. Amendola, M. A. Venneri, A. Biffi, E. Vigna, L. Naldini, Coordinate dual-gene transgenesis by lentiviral vectors carrying synthetic bidirectional promoters. *Nat. Biotechnol.* **23**, 108–116 (2005).
56. M. Bassani-Sternberg, S. Pletscher-Frankild, L. J. Jensen, M. Mann, Mass spectrometry of human leukocyte antigen class I peptidomes reveals strong effects of protein abundance and turnover on antigen presentation. *Mol. Cell. Proteomics* **14**, 658–673 (2015).
57. S. Feola, J. Chiaro, B. Martins, S. Russo, M. Fusciello, E. Ylösmäki, C. Bonini, E. Ruggiero, F. Hamdan, M. Feodoroff, G. Antignani, T. Viitala, S. Pesonen, M. Grönholm, R. M. M. Branca, J. Lehtiö, V. Cerullo, A novel immunopeptidomic-based pipeline for the generation of personalized oncolytic cancer vaccines. *eLife* **11**, e71156 (2022).
58. D. Gfeller, P. Guillaume, J. Michaux, H.-S. Pak, R. T. Daniel, J. Racle, G. Coukos, M. Bassani-Sternberg, The length distribution and multiple specificity of naturally presented HLA-I ligands. *J. Immunol.* **201**, 3705–3716 (2018).
59. J. Harrow, A. Frankish, J. M. Gonzalez, E. Tapanari, M. Diekhans, F. Kokocinski, B. L. Aken, D. Barrell, A. Zadissa, S. Searle, I. Barnes, A. Bignell, V. Boychenko, T. Hunt, M. Kay, G. Mukherjee, J. Rajan, G. Despacio-Reyes, G. Saunders, C. Steward, R. Harte, M. Lin, C. Howald, A. Tanzer, T. Derrien, J. Chrast, N. Walters, S. Balasubramanian, B. Pei, M. Tress, J. M. Rodriguez, I. Ezkurdia, J. Van Baren, M. Brent, D. Haussler, M. Kellis, A. Valencia, A. Reymond, M. Gerstein, R. Guigó, T. J. Hubbard, GENCODE: The reference human genome annotation for the ENCODE project. *Genome Res.* **22**, 1760–1774 (2012).
60. C. Soneson, M. I. Love, M. D. Robinson, Differential analyses for RNA-seq: Transcript-level estimates improve gene-level inferences. *F1000Research* **4**, 1521 (2015).

Acknowledgments: We thank L. Naldini (Ospedale San Raffaele Scientific Institute-OSR, Milano, IT; San Raffaele Telethon Institute for Gene Therapy HSR-TIGET) for providing 293 T packaging cells for LV production. We thank C. Covino (ALEMBIC facility, Ospedale San Raffaele Scientific Institute-OSR, Milano, IT) for providing help with the Incucyte data analysis, and C. Villa (FRACTAL facility, Ospedale San Raffaele Scientific Institute-OSR, Milano, IT) for the help with flow cytometry. We thank Intellia therapeutics for providing the CRISPR-Cas9 reagents for knocking out the endogenous TCR repertoire in T cells. **Funding:** This work was partially supported by Associazione Italiana per la Ricerca sul Cancro (AIRC-IG 18458 and AIRC 5 per Mille 22737), the Italian Ministry of Education, University and Research (PRIN 2017WC8499), and the Italian Ministry of Health and Alliance Against Cancer (Ricerca Corrente CAR T project: RCR-2019-23669115) to C.Bo.; by the Italian Ministry of Health (GR-2016- 02364847) to E.R., by an AIRC Fellowship to B.C.C. and F.Ma., and by an AIRC Investigator Grant (IG 22197) to L.V.; and by the Academy of Finland (grant nos. 309608 and 325222) to T.S. and M.H. **Author contributions:** F.Ma. participated in experimental design, performed the experiments, analyzed and interpreted data, and wrote the manuscript; L.S., S.B., M.N, F. Ma, and Z.M. performed experiments and interpreted data; D.A. interpreted flow cytometry data. C.T. and M.P. interpreted sequencing data and revised the manuscript. B.C. and E.T. were involved in the in vivo experiments. S.F., R.M.B., J.L., and V.C. performed and interpreted the PeptiChip analysis and revised the manuscript. C.Ba, B.C.C., A.P., M.T.L.S., M.S., L.V., and F.C. interpreted data and revised the manuscript; E.R. and C.Bo. participated in experimental design, analyzed and interpreted data, wrote and revised the manuscript. M.H. and T.S. supplied the PeptiChip platforms. **Competing interests:** C.Bo., B.C.C., E.R. F.Ma., and L.V. are inventors on different accepted patents on cancer immunotherapy and genome editing (Use of common g-chain cytokines for the visualization, isolation and genetic modification of memory T lymphocytes, Patent family PCT/IT2006/000600; Targeted disruption of T cell receptor genes using engineered zinc finger protein nucleases, Patent family US N. 12/927,292 and PCT/US2014/031360; WT1-TCRs, Patent family N. PCT/EP2018/060477 and N. PCT/EP2019/079916; Compositions and methods for immunotherapy, PCT/US2019/056399. Filed by San Raffaele Hospital). C.Bo. has been a member of Advisory Boards and a Consultant for Intellia Therapeutics, TxCell, Novartis, GSK, Allogene, Kite/Gilead, Miltenyi, Kiadis, Janssen and received research support from Intellia Therapeutics. L.V. received research support from GenDx and Moderna Therapeutics. S.F., V.C., and T.S. are inventors on the pending patent application PCT/EP2021/061981 (peptiChip Technology, filed by Helsinki University). The other authors declare no competing interests. **Data and materials availability:** All data needed to evaluate the conclusions in the paper are present in the paper and/or the Supplementary Materials. After publication, materials, data, and code will be provided by Ospedale San Raffaele pending scientific review and a completed material transfer agreement. Requests for materials, data, and code should be submitted to the corresponding authors (E.R., email: ruggiero.eliana@hsr.it; C. Bo., email: bonini.chiara@hsr.it). TCR sequencing data are deposited on Gene Expression Omnibus under the accession number GSE246651.

Submitted 22 January 2023
Accepted 2 November 2023
Published 1 December 2023
10.1126/sciadv.adg8014

ScienceAdvances

Harnessing T cell exhaustion and trogocytosis to isolate patient-derived tumor-specific TCR

Francesco Manfredi, Lorena Stasi, Silvia Buonanno, Francesca Marzuttini, Maddalena Noviello, Sara Mastaglio, Danilo Abbati, Alessia Potenza, Chiara Balestrieri, Beatrice Claudia Cianciotti, Elena Tassi, Sara Feola, Cristina Toffalori, Marco Punta, Zulma Magnani, Barbara Camisa, Elena Tiziano, Maria Teresa Lupo-Stanghellini, Rui Mamede Branca, Janne Lehtiö, Tiina M. Sikanen, Markus J. Haapala, Vincenzo Cerullo, Monica Casucci, Luca Vago, Fabio Ciceri, Chiara Bonini, and Eliana Ruggiero

Sci. Adv. **9** (48), eadg8014. DOI: 10.1126/sciadv.adg8014